8-3-2015

Residue Specific and Chirality Dependent Interactions between Carbon Nanotubes and Flagellin

Isaac Macwan

Zihe Zhao

Omar T. Sobh

Ishita Mukerji

Bhushan Dharmadhikari

See next page for additional authors

Peer Reviewed

Published Citation

Macwan, Isaac, Zihe Zhao, Omar T. Sobh, Ishita Mukerji, Bhushan Dharmadhikari, and Prabir K. Patra. "Residue Specific and Chirality Dependent Interactions Between Carbon Nanotubes and Flagellin." IEEE/ACM Transactions on Computational Biology and Bioinformatics. 13, no. 3 (2016): 541–48. https://doi.org/10.1109/TCBB.2015.2459696.

Authors

Isaac Macwan, Zihe Zhao, Omar T. Sobh, Ishita Mukerji, Bhushan Dharmadhikari, and Prabir K. Patra

Residue Specific and Chirality Dependent Interactions between Carbon Nanotubes and Flagellin

Isaac G. Macwan, Zihe Zhao, Omar T. Sobh, Ishita Mukerji, Bhushan Dharmadhikari, and Prabir K. Patra

Abstract—Flagellum is a lash-like cellular appendage found in many single-celled living organisms. The flagellin protofilaments contain 11-helix dual turn structure in a single flagellum. Each flagellin consists of four sub-domains - two inner domains (D0, D1) and two outer domains (D2, D3). While inner domains predominantly consist of α-helices, the outer domains are primarily beta sheets with D3. In flagellum, the outermost sub-domain is the only one that is exposed to the native environment. This study focuses on the interactions of the residues of D3 of an R-type flagellin with 5nm long chiral (5,15) and arm-chair (12,12) single-walled carbon nanotubes (SWNT) using molecular dynamics simulation. It presents the interactive forces between the SWNT and the residues of D3 from the perspectives of size and chirality of the SWNT. It is found that the metallic (arm-chair) SWNT interacts the most with glycine and threonine residues through van der Waals and hydrophobic interactions, whereas the semiconducting (chiral) SWNT interacts largely with the area of protein devoid of glycine by van der Waals, hydrophobic interactions, and hydrogen bonding. This indicates a crucial role that glycine plays in distinguishing metallic from semiconducting SWNTs.

Index Terms—Bacterial flagellum, flagellin domain, molecular dynamics, nanotube sorting, chirality

1 Introduction

One of the important aspects of the nano-bio-fabrication is the precise control of the atomic scale assembly by which organic and inorganic molecules are bound with each other. This requires insight into the detailed interactive forces that help forming such an assembly. Owing to rapidly changing conformations of proteins it is very challenging to experimentally quantify the interactions between proteins and nanomaterials hence molecular dynamics (MD) simulations can be efficiently utilized to study such interactions. A single unit cell of the flagellum is made up of protein flagellin (shown in Fig. 1) and in an 11-helix dual turn of a single flagellum, there are 11 such protofilaments [1]. The size of each flagellin is 140 Å in length and 110 Å in width. And each flagellin monomer is in a position perpendicular to the filament axis [2]. There are two major conformations of flagellin, L (Left) -type and R (Right) -type. During the normal bacterial motion called 'run', the flagellar filament forms a left-handed supercoil made of L-type and R-type flagellin. However, when the bacteria encounters an unfavorable condition such as increased oxygen levels or increased temperature, they often 'tumble' resulting in abrupt changes in their direction of motion. During such an event, the usual anti-clockwise motion of the flagellum is suddenly converted to clockwise. The sudden abruption in the flagellar motor twists the filaments, which loses their co-ordination converting the conformation of some L-type molecules to R-type [1] and convert temporarily the left-handed to right-handed supercoils. The molecular structure of both L-type and R-type flagellin monomers are already known from electron cryomicroscopy [1], [2]. Some of the investigations in the past based on MD simulations of the bacterial flagellum involved the motion of a rotating bacterial flagellum [3], the domain movement of the cap protein HAP2 from the viewpoint of flagellum growth [4] and the transportation of flagellin through the central channel for flagellar assembly [5]. Even though there are elegant reports on structure specific recognition and separation of SWNT using techniques such as DNA sequencing [6], [7], gel chromatography [8] and structure-discriminating surfactants [9], so far there is little to none information available on residue specific and chirality dependent interactions of SWNT and flagellin. Furthermore, previous studies involving MD simulations on the interaction of SWNTs and proteins involved protein domains such as YAP65WW [10], human serum albumin [11], signaling and regulatory protein domain SH3 [12] and also human blood serum proteins [13]. However, to the best of our knowledge, this is the first report on the use of MD

- *I.G. Macwan is with the Department of Biomedical Engineering, University of Bridgeport, 126 Park Avenue, Bridgeport, CT 06604. E-mail: imacwan@bridgeport.edu.*
- *Z. Zhao is with the Department of Computer Science, University of Bridgeport, 126 Park Avenue, Bridgeport, CT 06604. E-mail: zihezhao@my.bridgeport.edu.*
- *O.T. Sobh is with the Biology Department, University of Pennsylvania, 102 Leidy Laboratories, 433 S. University Avenue, Philadelphia, PA 19104. E-mail: osobh@sas.upenn.edu.*
- *I. Mukerji is with the Molecular Biology and Biochemstry Department, Wesleyan University, 45 Wyllys Avenue, Middletown, CT 06459. E-mail: imukerji@wesleyan.edu.*
- *B. Dharmadhikari is with the Department of Computer Science and Engineering, University of Bridgeport, 126 Park Avenue, Bridgeport, CT 06604. E-mail: bdharmad@my.bridgeport.edu.*
- *P.K. Patra is with the Departments of Biomedical and Mechanical Engineering, University of Bridgeport, 126 Park Avenue, Bridgeport, CT 06604. E-mail: ppatra@bridgeport.edu.*

Manuscript received 9 Mar. 2015; revised 7 July 2015; accepted 15 July 2015. Date of publication 0 . 0000; date of current version 0 . 0000.
For information on obtaining reprints of this article, please send e-mail to: reprints@ieee.org, and reference the Digital Object Identifier below.
Digital Object Identifier no. 10.1109/TCBB.2015.2459696

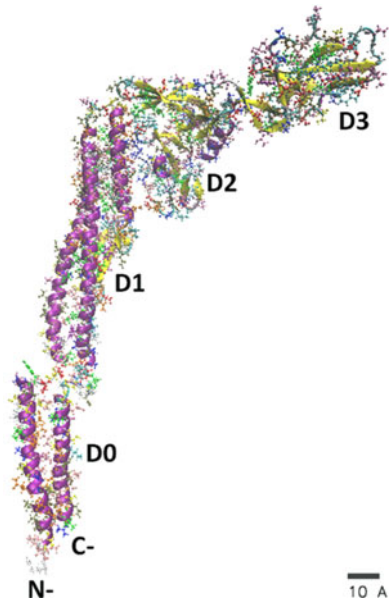

Fig. 1. Flagellin monomer portraying N- and C- terminals and the four domains D0, D1, D2, and D3. Domains D0 and D1 are predominantly made up of α-helics and domains D2 and D3 consists primarily of extended beta sheets.

simulations to study the residue specifc interactions between flagellin and SWNTs. The purpose of this work is to gain insights on the interactive behavior of flagellin with metallic (arm-chair) as well as semiconducting (chiral) SWNT from the perspectives of addressing the differences in the type and extent of interactive forces depending upon the chirality and size of the SWNTs. There are a few contradictory reports of the interaction of individual amino acids in general and glycine in particular with CNTs, where efforts were made to know the nature of binding between the amino acids and intrinsic as well boron-doped SWNTs [14], [15]. In this study, however, the role of glycine as a component of flagellin monomer is investigated by considering the way it interacts with (12,12) and (5,15) chirality SWNTs. This further leads to an interesting possibility that the position of glycine in the amino-acid sequence of flagellin might play a role in the way it interacts with different chirality nanotubes. The CNT-flagellin interation may pave the way for precise navigation and selective deposition of electronics. The larger goal of this research is to focus on the interaction of the magnetotactic bacteria with the carbon nanotubes by way of understanding as to how the flagellum of these bacteria would interact with CNTs. Furthermore, this gave an opportunity to understand as to why the growth of magnetotactic bacteria along with CNTs was successful in our culturing experiments and the intact motility of the bacterial cells in the presence of the CNTs validates the data that we find in this analysis that flagellin as a protein of the flagellum in the magnetotactic bacteria did not loose its function as a motility protein hence giving us some hints towards the toxicity of the CNTs to the magnetotactic bacteria as well.

2 Materials and Methods

MD simulations were prepared and analyzed using visual MD (VMD) [16] and are carried out using NAMD [17]. R-type flagellin filament pdb file (1UCU) was obtained from protein data bank (pdb) and an inbuilt nanotube builder plugin in VMD was used to create SWNTs of metallic (12,12) (m-CNT) as well as semiconducting (5,15) (s-CNT) nature with a length of 5nm. With simulations utilizing domain D3 (97 residues), both (12,12) m-CNT as well as (5,15) s-CNT were used and the simulations were carried out for a time period of 50 ns. In order to compare the changes in the conformation of D3, 50 ns runs were also performed on D3 alone with identical conditions as in the presence of CNTs. All simulations used the CHARMM force field [18] along with TIP3 water model [19] with a neutralizing salt concentration of NaCl for effective polarization of water molecules. Dell Studio XPS 9100 system with 8-core Intel i7 CPU and 16-core CUDA acceleration capability is utilized to perform all-atom simulations.

In each simulation, temperature was maintained at 300 K by Langevin thermostat and pressure of 1atm was maintained through Nose-Hoover Langevin-piston barostat with a period of 100 ps and a decay rate of 50 ps; periodic boundary conditions were assumed. Multiple time stepping was employed using an integration timestep of 2 fs, with short-range forces evaluated every time step and long range electrostatic forces evaluated every two timesteps. Short range forces were smoothed with a cutoff between 10 and 12 Å, while long range electrostatic forces were calculated using the particle-mesh Ewald algorithm. A salt strength just enough to neutralize the charge of the system was assumed. All-atom simulations of the interactions between D3 and SWNT and between R-type flagellin monomer and SWNT were performed in a periodic water box. The analysis plugins for root mean square deviation (RMSD) and NAMD energy were utilized to further investigate the nature of interactive forces and associated energies. TCL scripting language was utilized to query the different binding events in order to gain the insights about the binding interactions, number of atoms/residues involved and secondary structure conformations comparing the differences between binding of m-CNT and s-CNT with domain D3.

3 Results

Fig. 2 shows the ball and stick representations of the beginning and end of run for both m-CNT and s-CNT and provide a visual understanding of the nature of interaction between D3 and CNT (refer Table 1 for the exact number and type of residues).

A detailed RMSD analysis (Fig. 3) was performed to ensure stable protein conformation for both m-CNT and s-CNT interactions with D3 and was compared with D3 in the absence of the CNT for every frame upto the period of 50 ns (2,500 frames). It is seen that based on the stability of the domain D3, m-CNT is adsorbed at ~4ns (solid vertical line) whereas s-CNT is adsorbed at ~14 ns (dotted vertical line). This is comparable to the Fig. S2 showing the timeframe for the onset of adsorption (taken as less than 5 Å of the distance between the atoms of the D3 residues and CNT atoms) as early as 2.62 ns (frame 131) for m-CNT and 14.72 ns (frame 736) for s-CNT. The stability of the domain D3 after the adsorption is understood through reduced deviations in cases of m-CNT and s-CNT whereas in the absence of CNTs, D3 experiences uncertain increased deviations.

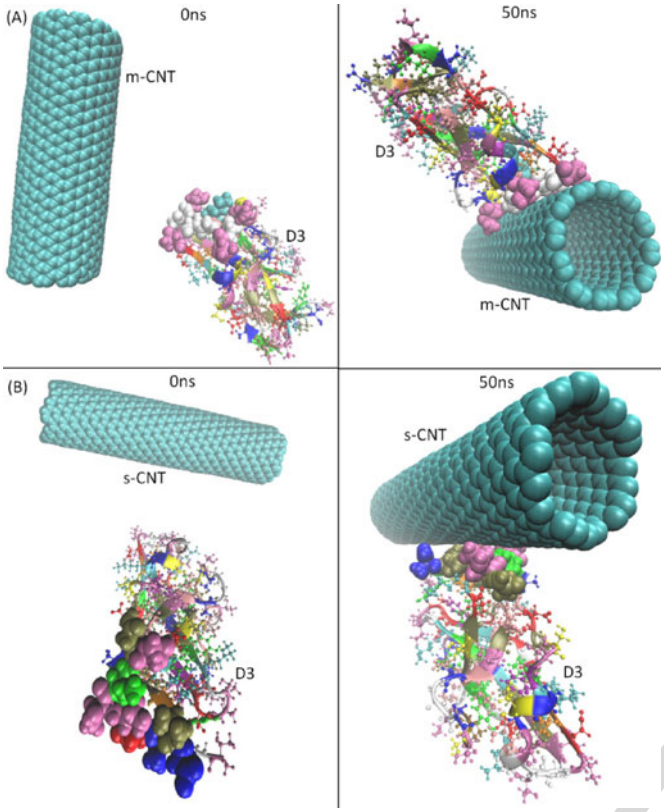

Fig. 2. Ball and stick representation of (A) m-CNT with D3 domain of flagellin before and after a simulation run of 50 ns, (Total atoms: 22,188). (B) s-CNT with D3 domain of flagellin before and after a simulation run of 50 ns. (Total atoms: 21,869). Water and neutralizing molecules of NaCl are not shown for clarity. The residues participating in the binding are shown using the VDW graphical representation.

The attraction events that occur during each timeframe for individual residues for 50 ns of time period are also captured through RMS deviation/fluctuation of the adsorbed residues (Figs. 4A, 4B, 4C) and a relative movement of the center of mass for D3 with respect to the CNTs is plotted

TABLE 1
Residues within 5Å of CNT Surface
(Criteria for Adsorption in the Present Study)

Type of CNT	Residue Name	Residue ID	Residue Type
m-CNT	Threonine	201, 207, 212, 239, 263	Polar uncharged
	Glycine	208, 210, 211, 237, 238, 260, 261	Aliphatic, non-polar
	Lysine	241	Basic, polar, positively charged
	Alanine	204, 262	Hydrophobic side-chain
	Leucine	209	Hydrophobic side-chain
	Serine	205, 248, 264	Polar, uncharged
s-CNT	Threonine	1, 193, 194, 252	Polar, uncharged
	Alanine	191, 196, 284	Hydrophobic side-chain
	Aspartic Acid	192. 198	Acidic, negatively charged side-chain
	Isoleucine	195	Hydrophobic side-chain
	Valine	283	Hydrophobic side-chain
	Asparagine	253, 280	Polar, uncharged
	Lysine	279	Basic, polar, positively charged

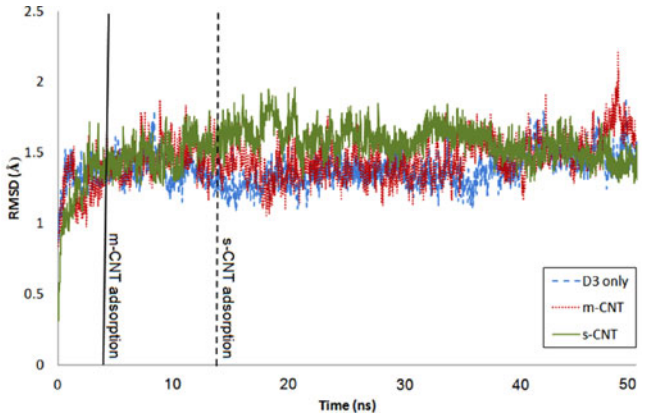

Fig. 3. RMSD for domain 3 in the absence and presence of m-CNT and s-CNT.

(Fig. 4D). It is found that in the presence of m-CNT (4A), the increased RMSD and RMSF (figures on the left and right of 4A) for the residues involved in the binding gets stabilized and there is a stable D3/m-CNT complex at the end of 50ns. Furthermore, Glycine plays a crucial role in binding with the m-CNT, which is also evident from Fig. S2 showing the presence of GLY starting about 3 ns until the end of the 50 ns. In comparison, for s-CNT there is no strong RMSD or RMSF seen indicating that s-CNT searched for an area of D3 that is devoid of GLY residue and in doing so ended up binding with D3 through strong hydrophobic and hydrogen bonds. It is also seen from the Fig. S2 that there is an absolute absence of GLY in case of s-CNT for all the 50 ns although about 15 residues of GLY are evenly distributed

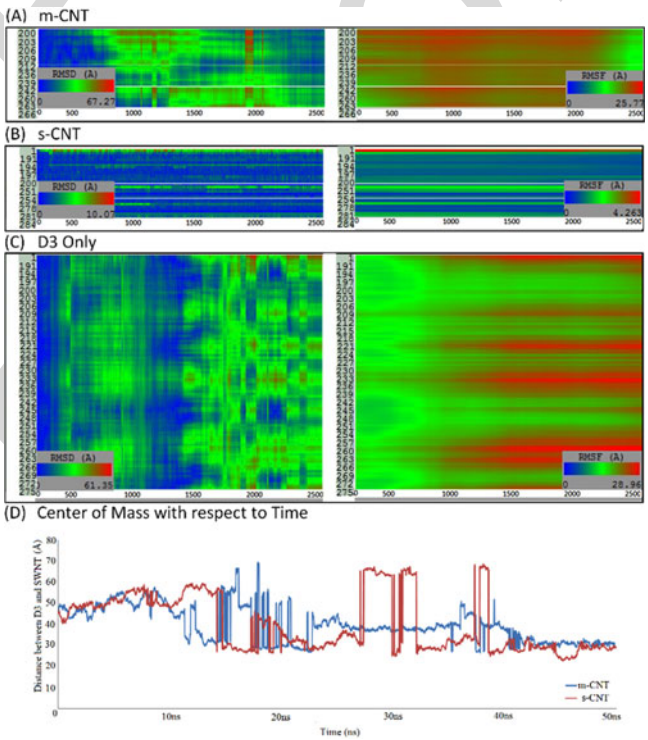

Fig. 4. Root mean square deviation (left)/ root mean square fluctuation (right) for the respective adsorbed residues onto (A) metallic (m-) CNT, and (B) semiconducting (s-) CNT. (C) RMS deviation (left)/ RMS fluctuation (right) for D3 in the absence of CNTs. (D) Center of mass variation of D3 with respect to m-CNT (blue) and s-CNT (red).

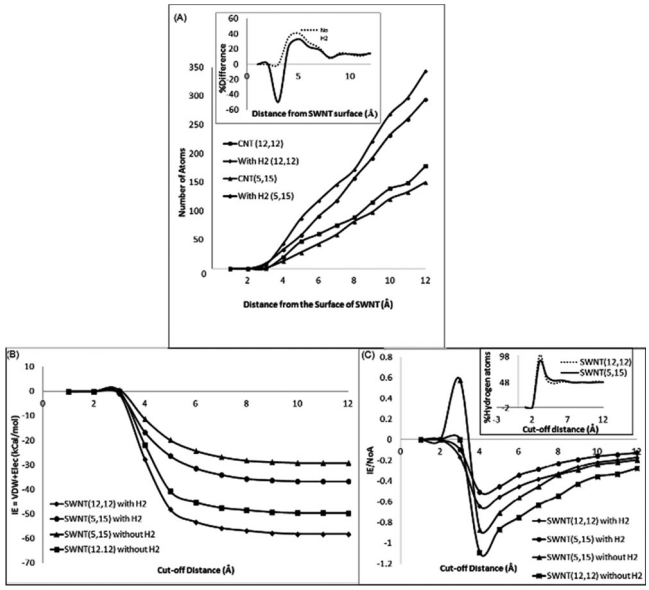

Fig. 5. (A) Plot showing number of atoms as a function of distance from the surface of SWNT for m-CNT and s-CNT including and excluding hydrogen. Inset: Difference in number of atoms including and excluding hydrogen between m-CNT and s-CNT. (B) Interaction energy as a function of cut-off distance for m- and s-CNT with and without hydrogen atoms. (C) Interaction energy/Number of atoms as a function of cut-off distance for m- and s-CNT with and without hydrogen atoms. Inset: Percentage hydrogen atoms as a function of cut-off distance.

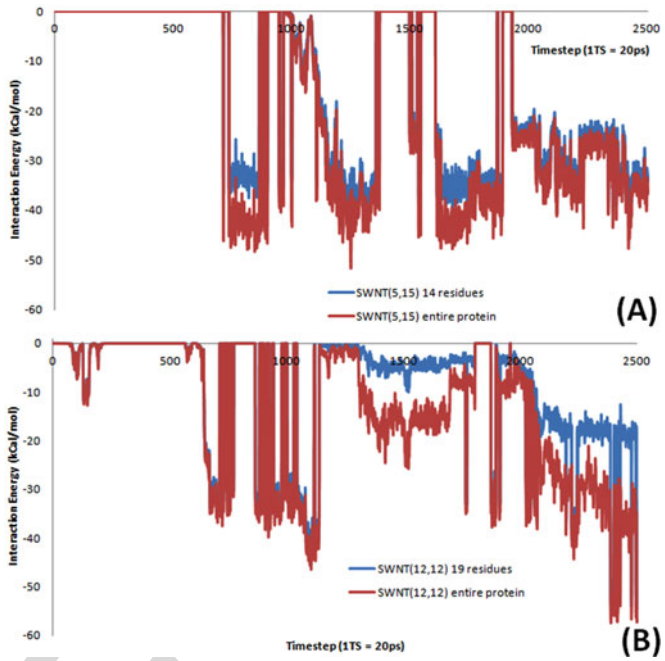

Fig. 6. Interaction energy as a function of time for (A) s-CNT showing the interaction solely based on the residues, whereas in (B) m-CNT showing the interaction energy arising also from long-range electrostat-ic energy from the remaining residues in D3.

on the D3 surface (Fig. S1). The Van Der Waals did play a role in binding of s-CNT as well but with an equal measure as that of hydropobic and hydrogen bonds. On the other hand, the instability of D3 in the absence of CNTs can be seen explicitly from Fig. 4C, where both RMSD and RMSF kept on increasing without a stable D3 state, which can be attributed to the interaction of D3 residues with salt ions and water molecules present in the media. Also from Fig. 4D, it is seen that the distance between the center of mass for both m-CNT as well as s-CNT and D3 is reduced from ~48 to ~28 Å, thereby confirming the attractive nature of the binding events. Both m-CNT and s-CNT were kept at ~20 Å away from D3 at approximately the same coordinates and hence this also confirms that the displacement of D3 is indeed towards m- and s-CNTs. The glitches are the result of rapidly changing conformations of the flagellin monomer as it is adsorbed on the CNT surface.

Number of atoms of D3 actively involved in the interaction phenomena are also found (Fig. 5A). The difference between the number of atoms interacting between CNT and D3 for m-CNT and s-CNT is consistent and it is further found that m-CNT binds with a slightly larger surface area as compared to s-CNT.

The interaction energy, IE (van der Waals + electrostatic) between m- as well as s-CNT and D3 was analyzed and IE as a function of cut-off distance was plotted (Figs. 5B, 5C). Based on this, the interaction per atom as a function of cut-off distance is also plotted and the effect of hydrogen atoms is analyzed (Fig. 5C).

In order to understand the reason behind a slightly stronger m-CNT binding with D3 compared to s-CNT, interaction energy analysis of all the residues involved in the interaction was done and was compared to the interaction energy of D3 as a whole with respect to m- and s-CNT (Fig. 6). Based on the electrostatic analysis (Fig. 7) of the D3 domain with respect to both m- and s-CNT, it can be seen that there is a distinct change in the electrostatic energy of D3 when it interacts with m-CNT whereas no such change is seen in case of s-CNT. For distances below 4 Å, hydrogen bonds were analyzed and it was found that the number of hydrogen bonds in s-CNT (Fig. 8B) are relatively more and having longer lifetimes compared to m-CNT (Fig. 8A).

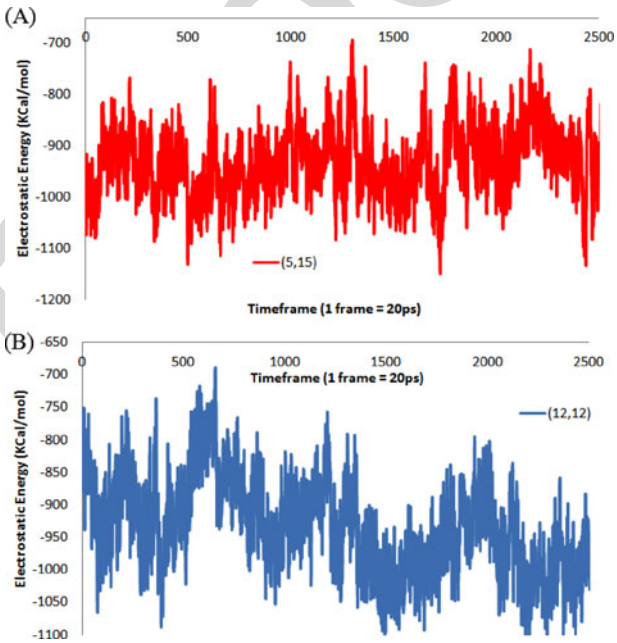

Fig. 7. Electrostatic energy of all the residues of D3 as a function of time for (A) s-CNT showing a constant average of –950 KCal/mol, whereas in (B) m-CNT showing the average electrostatic energy changing from ~900 to ~1000 KCal/mol around 25 ns (frame 1,250)

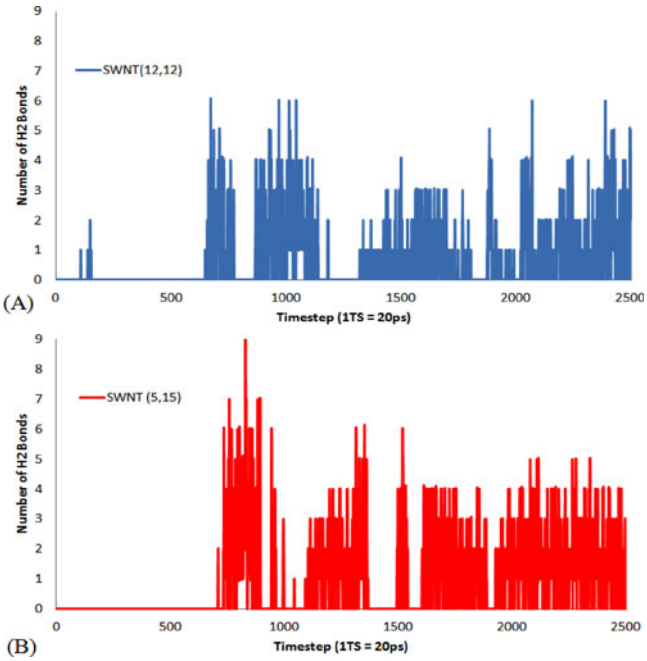

Fig. 8. Number of hydrogen bonds as a function of time for (A) m-CNT (blue) and (B) s-CNT (red).

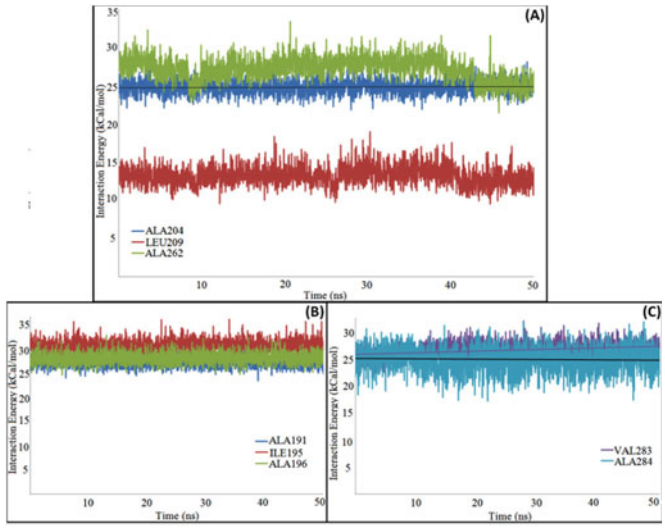

Fig. 9. Hydrophobic interactions between D3 and m-CNT (A) and between D3 and s-CNT (B), (C).

Apart from van der Waals and hydrogen bonding, hydrophobic interactions also played very important role in binding between CNT and flagellin. Out of all the residues that came in contact with both m-CNT and s-CNT, ALA204, LEU209 and ALA262 are the hydrophobic residues in case of m-CNT (Fig. 9A) and ALA191, ILE195, ALA196, VAL283 and ALA284 are the hydrophobic residues in case of s-CNT (Figs. 9B, 9C). The analysis revealed that Alanine plays a crucial role in hydrophobic interactions in case of m-CNT (25-28 kCal/mol) and both Alanine and Valine play significant roles in case of s-CNT (26-28 kCal/mol), thereby showing that s-CNT uses the hydrophobic interactions more effectively compared to m-CNT.

4 Discussion

MD is used to study the interactive forces between m- and s-CNT and it is found that residues GLY and THR are the most favorable ones that are adsorbed on the m-SWNT within the first 4 ns of the simulation run (Fig. 3). In contrast, it takes ~10 ns more with effective adsorption only after ~14 ns for D3 in the presence of s-CNT for the surface area devoid of glycine to be adsorbed. Both arm-chair (12,12) and chiral (5,15) carbon nanotubes were placed at approximately the same co-ordinates before the initial minimization and subsequent production runs. 15 Glycine (GLY) residues are evenly distributed on the D3 domain of the flagellin monomer (Fig. S1). Starting at the same co-ordinates, D3 took a different approach to bind with the arm-chair and chiral carbon nanotubes, which is evident from the Fig. S2, where even though GLY residues are evenly distributed over the surface, chiral carbon nanotube did not pick the surface of D3 that consisted of GLY. Also, from Fig. 1, it is confirmed that the residues participating in the binding between D3 and (5,15) nanotube are the ones located at the exact opposite side of the placement of the chiral nanotube unlike the (12,12) nanotube. Furthermore, looking at the S2, we confirm that out of the 15 GLY residues, none came closer to a distance less than 5Å showing any adsorption with the chiral nanotube. This fact alone indicates that due to the chiral twist of the nanotube, the semiconducting nature of the nanotube prevented any favorable interactive forces to exist between the chiral nanotube and GLY residues. In order to investigate whether the even distribution of GLY over the surface of the flagellin monomer does play a crucial role in the binding mechanism, additional 50 ns simulations were performed with three different orientations of the s-CNT with respect to the terminal end of the D3 domain—s-CNT above the terminal end of D3, S-CNT below the terminal end of D3 and s-CNT towards the terminal end of D3. It was found that indeed the surface of D3 devoid of GLY binds with a stable conformation with s-CNT (Fig. S5) whereas any presence of GLY is seen as an unstable ground for the s-CNT to bind with D3 (Figs. S3 and S4). Furthermore, the adsorption time (when any atom is at a distance <5Å from the surface of the nanotube) is determined primarily from the timeframes using a TCL script that determines the number of residues, type of residues and number of atoms at every timeframe for all 2,500 frames of the 50 ns run. In Fig. 3, the ~4 ns adsorption for (12,12) - metallic CNT and ~14 ns adsorption for (5,15) - semiconducting CNT was confirmed from the data shown in S2, where no residues came close to <5Å for (12,12) CNT until ~3 ns (frame 131) and in case of (5,15) carbon nanotube until ~14.72 ns (frame 736). This was also confirmed from the RMSD of D3 in the absence and presence of (12,12) and (5,15) CNTs as shown in Fig. 3, where the deflection of D3 is considered to point a stable complex of D3/CNT. The lesser the deflections, the more stable the complex.

Based on our previous report [20], it was found that in case of m-CNT (6,6) with a length of 1.2 nm, the effective adsorption takes place at ~5 ns comparable to the present case of m-CNT (12,12) having length of 5 nm. This indicates that the length of CNT, atleast in the metallic case, do not affect the adsorption time.

It is known that the interaction energy is part of the total potential energy according to the equation:

$$\text{Potential Energy (U)} = U_{\text{bonded}} + U_{\text{nonbonded}} \quad (1)$$

$$U_{\text{bonded}} = U_{\text{bonds}} + U_{\text{angles}} + U_{\text{dihedrals}} \quad (2)$$

$$U_{\text{nonbonded}} = \text{Interaction Energy} = U_{\text{vdw}} + U_{\text{elec}}. \quad (3)$$

Equation (2) is the bonding energy function that consists of energies composed of bonds, angles and dihedrals of the molecule under consideration. Similarly, Equation (3) is the non-bonding energy or interaction energy term that is composed of van der Waals and electrostatic energy between the two interacting entities. Out of these energies, the adsorption phenomena, which in this study is taken as the interactions at the length scales shorter than 5 Å, includes forces such as van der Waals, hydrogen bonding and hydrophobic interactions, whereas at scales larger than 5 Å, long range electrostatic forces are considered. It is found that even though D3 is adsorbed effectively both on m-CNT as well as s-CNT, it is bound to m-CNT with a slightly larger number of atoms (larger surface area) as compared to s-CNT (Fig. 5A) with an exception that at distance ~3 Å, the number of hydrogen atoms involved are more in case of s-CNT compared to m-CNT elucidating the reason for increased hydrogen bonds in case of s-CNT with longer life times (Fig. 8). The total interaction energy (van der Waals + electrostatic) was found to be more in case of m-CNT compared to s-CNT (Fig. 5B) and similarly, the interaction energy for each atom was found by taking a ratio of total interaction energy to the number of atoms within 5 Å of distance from the surface of the CNTs (Fig. 5C). This ratio gave significant insights into the optimal distance (~4 Å) at which the interaction energy per atom is the highest. Furthermore, a comparison between interaction energy for the residues within 5 Å distance to both m-CNT as well as s-CNT to thatdue to the rest of the D3 residues revealed that in case of s-CNT, there is no significant difference in the interaction energy values between the 14 adsorbed residues and rest of the residues of D3 indicating that these 14 residues solely govern the interaction phenomena (Fig. 6A). However, in case of m-CNT, there is a significant difference between the interaction energy values due to the 19 adsorbed residues and the rest of the D3 residues indicating that apart from van der Waals, hydrogen bonds and hydrophobic interactions that occur within the distances of 5 Å and below, there is another source of interaction energy that binds m-CNT and D3 (Fig. 6B). The potential source of interaction may be electrostatic, which due to its long distance nature would aid in the interactions between residues at distances larger than 5 Å and m-CNT. Interestingly, in case of s-CNT, such difference was not found indicating that s-CNT might not be interacting with D3 through electrostatic interactions. Hence, it is noted that the lack of interaction energy that s-CNT experiences due to the absence of electrostatic interactions is compensated through larger (and longer life time) hydrogen bonds and also through more hydrophobic residues playing an important role in interactions compared to m-CNT.

One of the challenges while studying the interactive force patterns through MD simulations is to differentiate between the binding events that occur when a protein comes in contact with a carbon nanotube especially with respect to its metallic and semiconducting chiralities. The role of the dominant geometric prtein sequences in D3 is crucial for differentiating the interactive binding with m- and s-CNT. For example, a glycine that is flanked by a threonine on one end and a tyrosine on the other may give rise to interaction events that are different from the viewpoint of the non-binding energy and chirality of the nanotube as compared to a glycine that is flanked by an asparagine on one end and glutamic acid on the other. This is precisely what is observed in Fig. 9A, where ALA262 residue has a slightly larger interaction energy and more fluctuations compared to ALA204 even though both are at the same distance from the surface of the m-CNT. The only difference between these two residues is the way they are flanked. ALA262 is flanked by GLY261 on one end and THR263 on the other end (both are the favored residues for m-CNT), whereas ALA204 is flanked by LYS203 on one end and SER205 on the other.

As a proof for the CNT-bacterial protein binding, ultraviolet circular dichroism (UV-CD) experiments were performed on Nanotubes, Bacteria and nanotube-bacteria mixed system. The variarion of protein secondary structure (as shown in supplementary figure S3, which can be found on the Computer Society Digital Library at http://doi.ieeecomputersociety.org/10.1109/TCBB.2015.2459696) in case of only the bacteria and the CNT-bacteria is observed with in the wave length range of 250-275 nm in the spectral pattern. This shows the binding of the bacterial proteins with CNT.

Finally, in the presence of m-CNT, the residues undergo large fluctuations initially resulting in large RMSD but these fluctuations die down as the m-CNT form stable complex with the D3 (Fig. 4A). However, in case of D3 alone, these fluctuations do not die down, rather they continue to increase (Fig. 4C) validating a stable binding in case of m-CNT. On the other hand, in case of s-CNT, there are little RMSF signatures (Fig. 4B) indicating that due to the semiconducting nature of the CNT, the optimum potential for utilizing electrostatic interactions has not yet been reached.

5 Conclusion

MD simulations are performed on an isolated domain D3 of flagellin monomer in the presence of both metallic (12,12) as well as semiconducting (5,15) SWNT. Based on the simulation runs for 50 ns, it is observed that SWNT most favorably interacts with GLY as well as THR residues. Furthermore, m-SWNT stabilizes twice as fast as semiconducting SWNT as evident from the RMSD analysis. Other non-binding interactions such as van der Waals, hydrophobic interactions and hydrogen bonding confirm stable binding between D3 and m-CNT as well as s-CNT. Metallic and semiconducting carbon nanotubes are found to interact in a different manner with flagellin, which may provide a basis for efficient sorting of CNTs based on the presence or absence of glycine residue. It is also found that electrostatic interactions play a significant role in binding phenomena in case of metallic but not in case of semiconducting carbon nanotubes for pristine CNTs. Glycine plays a dominant role

in the interaction mechanism, where metallic carbon nanotubes bind with D3 in as small as ~4 ns placed at an initial distance of ~20 Å. On the contrary, semiconducting carbon nanotubes take ~14 ns for the onset of D3 adsorption and totally avoid the vicinity of glycine indicating that the chiral twists of the CNT may have a threshold voltage constraint for the onset of the electrostatic interactions.

Acknowledgments

I. G. Macwan and P. K. Patra are noted as the corresponding authors for this work. IGM, PKP and BD acknowledge Brookhaven National Lab's (BNL) supercomputational facility for performing part of the NAMD work.

References

[1] S. Maki-Yonekura, K. Yonekura, and K. Namba, "Conformational change of flagellin for polymorphic supercoiling of the flagellar filament," *Nat. Struct. Mol. Biol.*, vol. 17, no. 4, pp. 417–422, Apr. 2010.

[2] K. Yonekura, S. Maki-Yonekura, and K. Namba, "Complete atomic model of the bacterial flagellar filament by electron cryomicroscopy," *Nature*, vol. 424, no. 6949, pp. 643–650, Aug. 2003.

[3] A. Arkhipov, P. L. Freddolino, K. Imada, K. Namba, and K. Schulten, "Coarse-grained molecular dynamics simulations of a rotating bacterial flagellum," *Biophys. J.*, vol. 91, no. 12, pp. 4589–4597, Dec. 2006.

[4] S. Maki-Yonekura, K. Yonekura, and K. Namba, "Domain movements of HAP2 in the cap-filament complex formation and growth process of the bacterial flagellum," *Proc. Nat. Acad. Sci. USA*, vol. 100, no. 26, pp. 15528–15533, Dec. 2003.

[5] D. E. Tanner, W. Ma, Z. Chen, and K. Schulten, "Theoretical and computational investigation of flagellin translocation and bacterial flagellum growth," *Biophys. J.*, vol. 100, no. 11, pp. 2548–2556, Jul. 2011.

[6] X. Tu, S. Manohar, A. Jagota, and M. Zheng, "DNA sequence motifs for structure-specific recognition and separation of carbon nanotubes," *Nature*, vol. 460, no. 7252, pp. 250–253, Jul. 2009.

[7] M. Zheng, A. Jagota, M. S. Strano, A. P. Santos, P. Barone, S. G. Chou, B. A. Diner, M. S. Dresselhaus, R. S. McLean, G. B. Onoa, G. G. Samsonidze, E. D. Semke, M. Usrey, and D. J. Walls, "Structure-based carbon nanotube sorting by sequence-dependent DNA assembly," *Science*, vol. 302, no. 5650, pp. 1545–1548, Nov. 2003.

[8] H. Liu, D. Nishide, T. Tanaka, and H. Kataura, "Large-scale single-chirality separation of single-wall carbon nanotubes by simple gel chromatography," *Nat. Commun.*, vol. 2, p. 309, Jan. 2011.

[9] M. S. Arnold, A. A. Green, J. F. Hulvat, S. I. Stupp, and M. C. Hersam, "Sorting carbon nanotubes by electronic structure using density differentiation," *Nat. Nanotechnol.*, vol. 1, no. 1, pp. 60–65, Oct. 2006.

[10] Q.-T. Dou, G.-H. Zuo, and H.-P. Fang, "Interaction between a functionalized single-walled carbon nanotube and the YAP65WW protein domain: A molecular dynamics simulation study," *Chin. Phys. Lett.*, vol. 29, no. 6, p. 068701, Jun. 2012.

[11] J.-W. Shen, T. Wu, Q. Wang, and Y. Kang, "Induced stepwise conformational change of human serum albumin on carbon nanotube surfaces," *Biomaterials*, vol. 29, no. 28, pp. 3847–3855, Oct. 2008.

[12] M. Ahmad, W. Gu, and V. Helms, "Mechanism of fast peptide recognition by SH3 domains," *Angew. Chem. Int. Ed.*, vol. 47, no. 40, pp. 7626–7630, Jan. 2008.

[13] C. Ge, J. Du, L. Zhao, L. Wang, Y. Liu, D. Li, Y. Yang, R. Zhou, Y. Zhao, Z. Chai, and C. Chen, "Binding of blood proteins to carbon nanotubes reduces cytotoxicity," *Proc. Nat. Acad. Sci. USA.*, vol. 108, no. 41, pp. 16968–16973, Oct. 2011.

[14] A. Mavrandonakis, S. C. Farantos and G. E. Froudakis, "Glycine interaction with carbon nanotubes: An ab initio study," *J. Phys. Chem. B*, vol. 110, no. 12, pp. 6048–6050, Mar. 2006.

[15] W. Sun, Y. Bu, and Y. Wang, "Interaction between glycine/glycine radicals and intrinsic/boron-doped (8,0) single-walled carbon nanotubes: A density functional theory study," *J. Phys. Chem. B*, vol. 112, no. 48, pp. 15442–15449, Dec. 2008.

[16] W. Humphrey, A. Dalke, and K. Schulten, "VMD: Visual molecular dynamics," *J. Mol. Graph.*, vol. 14, no. 1, pp. 33–38, Feb. 1996.

[17] J. C. Phillips, R. Braun, W. Wang, J. Gumbart, E. Tajkhorshid, E. Villa, C. Chipot, R. D. Skeel, L. Kalé, and K. Schulten, "Scalable molecular dynamics with NAMD," *J. Comput. Chem.*, vol. 26, no. 16, pp. 1781–1802, Dec. 2005.

[18] A. D. MacKerell, D. Bashford, R. L. Dunbrack, J. D. Evanseck, M. J. Field, S. Fischer, J. Gao, H. Guo, S. Ha, D. Joseph-McCarthy, L. Kuchnir, K. Kuczera, F. T. K. Lau, C. Mattos, S. Michnick, T. Ngo, D. T. Nguyen, B. Prodhom, W. E. Reiher, B. Roux, M. Schlenkrich, J. C. Smith, R. Stote, J. Straub, M. Watanabe, J. Wiórkiewicz-Kuczera, D. Yin, and M. Karplus, "All-atom empirical potential for molecular modeling and dynamics studies of proteins," *J. Phys. Chem. B*, vol. 102, no. 18, pp. 3586–3616, Apr. 1998.

[19] W. L. Jorgensen, J. Chandrasekhar, J. D. Madura, R. W. Impey, and M. L. Klein, "Comparison of simple potential functions for simulating liquid water," *J. Chem. Phys.*, vol. 79, no. 2, p. 926, Jul. 1983.

[20] I. Macwan, Z. Zhao, O. Sobh, and P. Patra, "A flagellum based study of semiconductor nanofabrication through magnetotaxis," in *Proc. 36th Annu. Int. Conf. IEEE Eng. Med. Biol. Soc.*, 2014, pp. 2777–2780.

Isaac G. Macwan received the bachelor's of engineering degree in electrical engineering from the University of Pune, India, in 2005. He received the MS degree in electrical engineering and the PhD degree in computer science and engineering from the University of Bridgeport in 2008 and 2014, respectively. He is a postdoctoral researcher with the Department of Biomedical Engineering, University of Bridgeport. His research interests include directed self assembly strategies and their applications in bioelectronics through the use of micro-organisms and fundamental investigations pertaining to the interface between organic and inroganic materials.

Zihe Zhao received the MS degree in biomedical engineering from the University of Bridgeport in 2012. He is currently working toward the MS degree in the Department of Computer Science, University of Bridgeport. His research interestes include microbiology focusing on the use of novel micro-organisms for biomedical engineering applications.

Omar T. Sobh is a full time senior at the University of Pennsylvania, and will be graduating in May of 2015 with a bachelor's of arts degree in biology. After graduation, he will be attending medical school as a doctor of medicine candidate with an expected completion date of 2019. His research area focuses on nanomaterials and was featured in the 2014 IEEE EMBC conference, 2014 ASEE Zone 1 Conference, and 2014 BMES conference.

Ishita Mukerji is a professor in the Department of Molecular Biology and Biochemistry. Her research focuses on using spectroscopic methods to elucidate the mechanisms of recognition and binding in protein-DNA interactions. Using a combination of fluorescence and Raman spectrospic tools, her work also centers on the studies on the proteins that play an important role in controlling gene expression and packaging DNA.

Bhushan Dharmadhikari received the BS degree in electronics and telecommunications from Bharati Vidyapith, Pune, India, and the MS degree in electrical engineering from the University of Bridgeport, CT. He is a recent PhD graduate from the Department of Computer Science and Engineering, University of Bridgeport. His major research interests are in computational bio engineering.

Prabir K. Patra received the PhD degree in materials science and engineering. He is an associate professor and chair in the Biomedical Engineering Department, University of Bridgeport. He is also an associate professor in the Mechanical Engineering Department. He is a member of the BMES, IEEE, and MRS. The focus of his research is to understand the fundamentals of biophysical science processes at a nano-scale and apply their underlying principles to develop hybrid material structure, properties, and arrangement through growth and modification for novel biomedical engineering applications.